IEEE Access
Multidisciplinary | Rapid Review | Open Access Journal

Date of publication xxxx 00, 0000, date of current version xxxx 00, 0000.

Digital Object Identifier 10.1109/ACCESS.2017.Doi Number

Performance Enhancement of Gulf of El Zayt Wind Farm in Egypt using a Novel Optimized Seconded Sliding Mode Control

Mohamed Ebeed[1], Nagwa Elbadry[1], Khairy Sayed [1], Ahmed Rashad [2], Sulaiman Z. Almutairi [3], Ahmed. T. Hachemi [4], Emad A. Mohamed [3,5], and Shazly A. Mohamed [6]

[1]Department of Electrical Engineering, Faculty of Engineering, Sohag University, Sohag 82524, Egypt
[2]Ministry of Electricity and Energy, Egypt
[3]Department of Electrical Engineering, College of Engineering, Prince Sattam bin Abdulaziz University, Al Kharj 16278, Saudi Arabia
[4]Electrical Engineering Laboratory, University of Kasdi Merbah, Ouargla 30000, Algeria
[5]Department of Electrical Engineering, Faculty of Engineering, Aswan University, Aswan 81542, Egypt
[6]Electrical Engineering Department, Faculty of Engineering, South Valley University, Qena 83523, Egypt

Corresponding author: Emad A. Mohamed (e.younis@psau.edu.sa).

This project is sponsored by Prince Sattam bin Abdulaziz University (PSAU) as part of funding for its SDG Roadmap Research Funding Programme project number PSAU-2023-SDG-121

ABSTRACT Gulf of El Zayt wind farm is one of the giant projects for wind stations in Egypt, as its production is expected to reach up to 580 MW. Sliding Mode Control (SMC) is characterized by its ability to achieve rapid control of systems which suffer from the impact of uncertainty variables. This paper presents an improved method to enhance the effect of Seconded Order Sliding Mode Control (SSMC) on the applied systems. This improved method consists of a combination of the SSMC and proportional integral controller (PI) which is named as an optimized Seconded Order SMC-PI Control (OSSMC-PI). The Slime Mould Algorithm (SMA) and the particle swarm optimization (PSO) methods are applied to assign the optimal gains of proposed OSSMC-PI controller. To clear up the achievement of this improved method, its impact on the performance of Gulf of El Zayt wind farm stage one - 120 MW (GZWF-120) during a three-phase fault is compared with the impact of different control technologies such as the proportional integral controller (PI), optimized PI controller and PI-SMC controller the performance of GZWF-120. The system performance is enhanced considerably with the application of the suggested OSSMC-PI controller compared to the classical SM controller and PI controller.

INDEX TERMS Wind energy, Sliding mode control, SMA optimization, PI controller, PSO.

List Of Abbreviation

SMC	Sliding Mode Control
SSMC	Seconded Order Sliding Mode Control
PI	Proportional integral controller
OSSMC-PI	Optimized Seconded Order SMC-PI Control
SMA	Slime Mould Algorithm
PSO	Particle swarm optimization
GZWF	Gulf of El Zayt wind farm
DFIGs	Doubly fed induction generators
WT	Wind turbine
SM	Sliding mode
ANFIS	Adaptive neuro-fuzzy inference system
IIR	Infinite impulse response
K_p	Proportional gain
K_i	Integral gain
α	Coefficient which is based on the fixed parameters of DFIG
THD	Total harmonic distortion
SOSM	Second order sliding mode
GSC	Grid side converter
RSC	Rotor side converter
V	Wind speed
R	Turbine radius
ρ_{air}	Air density
C_p	WT's aerodynamic efficiency
λ	Tip velocity ratio
β	Angle of blade pitch
ω_t	Shaft of the generator
T_m	Mechanical torque
P_{WT}	Wind turbine output power
d, q	Park reference frame

v_{ds}	Direct axis of the stator voltage
v_{qs}	Quadrature axis of the stator voltage
i_{ds}	Direct axis of the stator current
i_{qs}	Quadrature axis of the stator current
V_{dr}	Direct axis of the rotor voltage
V_{qr}	Quadrature axis of the rotor voltage
i_{dr}	Direct axis of the rotor current
i_{qr}	Quadrature axis of the rotor current
φ_{ds}	Direct axis of the stator flux
φ_{ds}	Quadrature axis of the stator flux
φ_{dr}	Direct axis of the rotor flux
φ_{qr}	Quadrature axis of the rotor flux
R_s	Resistance of the stator
R_r	Resistances of the rotor
ω_s	The synchronous angular speeds
ω_r	The rotor angular speeds
M	The mutual inductance
T_{em}	Electromagnetic torque
P_s	The active power of the stator
P_r	The reactive power of the stator
g	The slip range
V_{gconv}	The converter of grid voltage
V_{rconv}	The converter of rotor voltage
P_{ref}	The reference of the active power
F	Disturbance
P_{opt}	The optimum power
e_p	The error power function
S	Switching function
DC	Direct current
AC	Alternating current
P_F	The measured power during disturbance
V_F	The measured AC voltage during disturbance
V_{DC-F}	The measured DC voltage during disturbance
e_{p-rsc}	The error power signal of the rotor side converter
e_{v-rsc}	The error of AC voltage of the rotor side converter
$e_{vdc-gsc}$	The error of DC voltage of the grid side converter
V_{d-gsc}	Direct component of the voltage of grid side converter
V_{q-gsc}	Quadratic components of the voltage of grid side converter
V_{dq-gsc}	The direct and quadratic components of the voltage of grid side Converter
η	Acceleration constant
V_r	The rated wind speed
V_{out}	The cut-out wind speed
V_{in}	The cut-in wind speed
T_{max}	The maximum iteration number
SI	The sorting of the objective function
$h_A,\ h_B$	Random vectors from the populations
bF	The best objective function
wF	The worst objective function
DL	The best objective function
lb	The lower limit of the search range
ub	The upper limit of the search range
z	Constant value
h_i	The populations of the PSO
V_i	The populations velocity
G	The best global population is determined
CPU	Central processing unit
PC	Personal computer
V_{ref}	Reference voltage
Q_{wf}	Reactive power injected from the DC bus of wind farm
Q_{sys}	System reactive power

I. INTRODUCTION

Wind energy is highly incorporated types of renewable energies sources to the electric grids. Wind energy sources are the most competitive energy sources compared to conventional energy from a techno, economic and eco-friendly perspective. Wind power growth is about 27% has been experienced among all renewable energy sources in 2022. In 2023, it was predicted that 14% of the supplied energy comes from wind-based energy system[1] [2]. The Doubly fed induction generators (DFIGs) are wieldy incorporated in modern power systems due to their high control capability and wide speed operation [3]. In addition to that the DFIG cost is less than full-scale power converter wind turbines (WTs)due to the reduction in the low costs of its inverter which is less than the full-scale WT's inverter by (25–30%) [4].

The DFIG over several advantages compared to full-scale converter wind energy system but it is very sensitive for any disturbance in the electric grid. Thus, it is mandatory to provide effective and robust control methods for the DFIG to improve its performance during grid disturbances. The conventional proportional–integral (PI) controller was employed to provide the required control ability for the DFIG [5-7].

The PI controller is simple to be applied to provide the control ability of the DFIG. However, it can't provide the high precision control ability for nonlinear dynamic disturbances or states. Thus, due to the limitation of the conventional PI the sliding mode (SM) controller is wildly implemented for the fault ride-through or to improve the performance of the DFIG where a nonlinear sliding-mode control was suggested for the active and the reactive powers control of the DFIG in which the SM was utilized to determine the rotor control voltage without extra current control loops [8]. In [9], SM controller was employed for regulation the dc-link voltage and power control. A SM control with new exponential reaching law was present-ed for reduction the chattering phenomenon of the DFIG under variation of wind speed [10]. A feedback linearization methodology and SM controller was proposed to diminish

the sub-synchronous control interaction of the DFIG with series compensator [11]. A modified Super-Twisting SM control was presented and implemented to the wind energy system for diminishing the total harmonic distortion (THD) and improving the power system performance during the faults [12]. In [13-16], the second order SM (SOSM) controller was employed for maximizing the output power of the DFIG under different states. A fractional order SM control was proposed to provide the efficient control abilities for the maximum power point tracking of the DFIG [17]. The SOSM control based on damping controller was proposed for utilization of the reactive power capability to emphasis the stability of the power system during the disturbances [18]. In [19], a SOSM base on Super-Twisting ANFIS was proposed for maximizing the captured power from the DFIG to overcome the chattering problem.

Slime mould algorithm (SMA) is robust technique that mimics the propagation of slime mould [20]. The SMA was applied for optimizing several problems like image segmentation [21, 22], photovoltaic parameters [23, 24], economic emission dispatch [25], medical classification [26], feature selection [27], proportional derivative integral controller design [28], optimal power flow [29], design of digital IIR filter [30], mobile robots [31].

In this work, the ability of SMC is employed to control DFIG converters regardless of unexpected changes in system parameters. As it can be seen in a literature review, SMC depends on a coefficient (α) which is based on the fixed parameters of DFIG. This paper presents a modification to SSMC based on determining the optimal value of (α) using different techniques of optimization. The paper named this modified SSMC with Optimized Seconded Order SMC-PI Control (OSSMC-PI). Also, different techniques of optimization are used to reach the optimized PI gains K_p (and K_i) not only in the converter of the rotor side but also in the converter of the grid side using (K_p and K_i). OSSMC-PI is applied to Gulf of El Zayt wind farm in order to handle the unsatisfactory performance of Gulf of El Zayt wind farm especially disconnection from the electrical network during fault conditions. To demonstrate the effectiveness of OSSMC-PI on the performance of Gulf of El Zayt wind farm; the performance of Gulf of El Zayt wind farm is handled using 6 different control cases and comparison between the results to get the best case.

The paper contributions are listed as follows:

- A new optimized Seconded Order SMC-PI Control (OSSMC-PI) is proposed for DFIG's performance enhancement.
- Assessing the performance of a real Gulf of El Zayt wind farm energy conversion system with integration of the proposed controller under the fault's occurrence.
- The optimal gains of the proposed OSSMC-PI are assigned optimally using slim molded algorithm and the obtained results are compared to the PSO.
- The performance of the OSSMC-PI is compared to the classical SMC and PI.

The remaining sections in this manuscript are outlined as follows: Section 2 gives a description of DFIG modelling and its construction. Section 3 illustrates the conventional control of DFIG as well as the Seconded Order SMC and the suggested controller. Section 4 describes the configuration of the Gulf of El Zayt wind farm. Section 5 gives an overview of the SMA and the PSO methods. Section 6 lists the numerical simulation and the corresponding discussion while the conclusion is outlined in section 7.

II. CONFIGURATION AND MODELING OF THE DFIG

The main construction of the DFIG is shown in Figure 1 where it consists of wound rotor induction generators which are coupled with the blade of the WT via gear box. The stator is connected to the electrical network directly while the rotor is linked to the electric system via the grid side converter (GSC) and the rotor side converter (RSC) are connected together in back-to-back configuration.

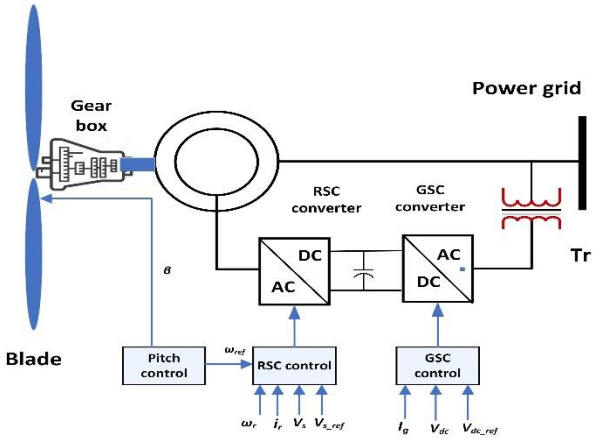

FIGURE 1. Construction of the DFIG.

A. MODELING OF THE WIND TURBINE (WT)

The aerodynamic generated power of the WT can be assigned using (1) as follows [32]:

$$P_{WT} = \frac{1}{2}\rho_{air}\,\pi R^2 C_p(\lambda,\beta)V^3 \tag{1}$$

where V, R, ρ_{air}, C_p, λ and β represent the wind speed, the turbine radius, the air density, WT's aerodynamic efficiency, the tip velocity ratio and the angle of blade pitch which can be expressed as follows:

$$\lambda = \frac{\omega_t R}{V} \tag{2}$$

The produced mechanical torque by the WT can be calculated as follows [33]:

$$T_m = \frac{P_{WT}}{\omega_t} = \frac{1}{2\lambda^3}\rho_{air}\pi R^5 C_p(\lambda,\beta)\omega_t^2 \tag{3}$$

where ω_t refers to the shaft of the generator.

The DFIG dynamic model is represented in Park reference frame (d, q) using the following equations [34]:

$$v_{ds} = R_s i_{ds} + \frac{d\varphi_{ds}}{dt} - \omega_s \varphi_{qs} \tag{4}$$

$$v_{qs} = R_s i_{qs} + \frac{d\varphi_{qs}}{dt} + \omega_s \varphi_{ds} \quad (5)$$

$$v_{dr} = R_r i_{dr} + \frac{d\varphi_{dr}}{dt} - (\omega_s - \omega_r)\varphi_{qr} \quad (6)$$

$$v_{qr} = R_r i_{qr} + \frac{d\varphi_{qr}}{dt} + (\omega_s - \omega_r)\varphi_{dr} \quad (7)$$

$$\varphi_{ds} = L_s i_{ds} + M i_{dr} \quad (8)$$

$$\varphi_{qs} = L_s i_{qs} + M i_{qr} \quad (9)$$

$$\varphi_{qr} = L_r i_{qr} + M i_{qs} \quad (10)$$

$$\varphi_{dr} = L_r i_{dr} + M i_{ds} \quad (11)$$

$$T_{em} = 1.5p\left(\varphi_{ds} i_{qs} - \varphi_{qs} i_{ds}\right) \quad (12)$$

where v_{ds}, and v_{qs} are the $d-$ and $q-$ axis of the stator voltage's components. i_{ds} and i_{qs} are the $d-$ and $q-$ axis of the stator current's components. V_{dr}, and V_{qr} are the $d-$ and $q-$ axis of the rotor voltage's components. i_{dr} and i_{qr} are the $d-$ and $q-$ axis of t

he rotor current's components. φ_{ds} and φ_{qs} are the $d-$ and $q-$ axis of the stator flux's components. φ_{dr} and φ_{qr} are the $d-$ and $q-$ axis of the rotor flux's components, respectively. R_s and R_r represent the resistances of the stator and the rotor, respectively. ω_s, and ω_r are the synchronous and the rotor angular speeds, respectively. M is the mutual inductance. T_{em} refers to electromagnetic torque. The DFIG's stator resistance is neglected while the stator flux is constant and aligned with the $d-$ axis [35]. Thus, $\varphi_s = \varphi_{ds}$ and $\varphi_{qs} = 0$ and the previous equations of the be modified as follows:

$$v_{ds} \approx 0 \quad (13)$$

$$v_s = v_{qs} \approx \omega_s \varphi_s \quad (14)$$

$$\varphi_s = L_s i_{ds} + M i_{dr} \quad (15)$$

$$0 = L_s i_{qs} + M i_{qr} \quad (16)$$

$$T_{em} = -\frac{3}{2} p \frac{M}{L_s} \varphi_s i_{qr} \quad (17)$$

Likewise, the rotor voltages can be represented using (18) and (19).

$$V_{dr} = R_r i_{dr} + \left(L_r - \frac{M^2}{L_s}\right)\frac{di_{dr}}{dt} - g\omega_s\left(L_r - \frac{M^2}{L_s}\right) i_{qr} \quad (18)$$

$$V_{qr} = R_r i_{qr} + \left(L_r - \frac{M^2}{L_s}\right)\frac{di_{qr}}{dt} + g\omega_s\left(L_r - \frac{M^2}{L_s}\right) i_{dr} + g\frac{Mu_s}{L_s} \quad (19)$$

where g refers to the slip range. The stator active and reactive powers are represented using (20) and (21).

$$P_s = \frac{3}{2}\left(v_{ds} i_{ds} + v_{qs} i_{qs}\right) \quad (20)$$

$$Q_s = \frac{3}{2}\left(v_{qs} i_{ds} - v_{ds} i_{qs}\right) \quad (21)$$

1) THE CONTROL MODES OF THE DFIG

a) The conventional Control mode

As it is known DFIG is composed of two converters including the GSC and the RSC as shown in Figure 2 (a). The converter of grid side controls produces the grid voltage (V_{gconv}) as shown in Figure 2 (b) while the converter of rotor side controls produces the rotor voltage (V_{rconv}) as displayed in Figure 2 (c).

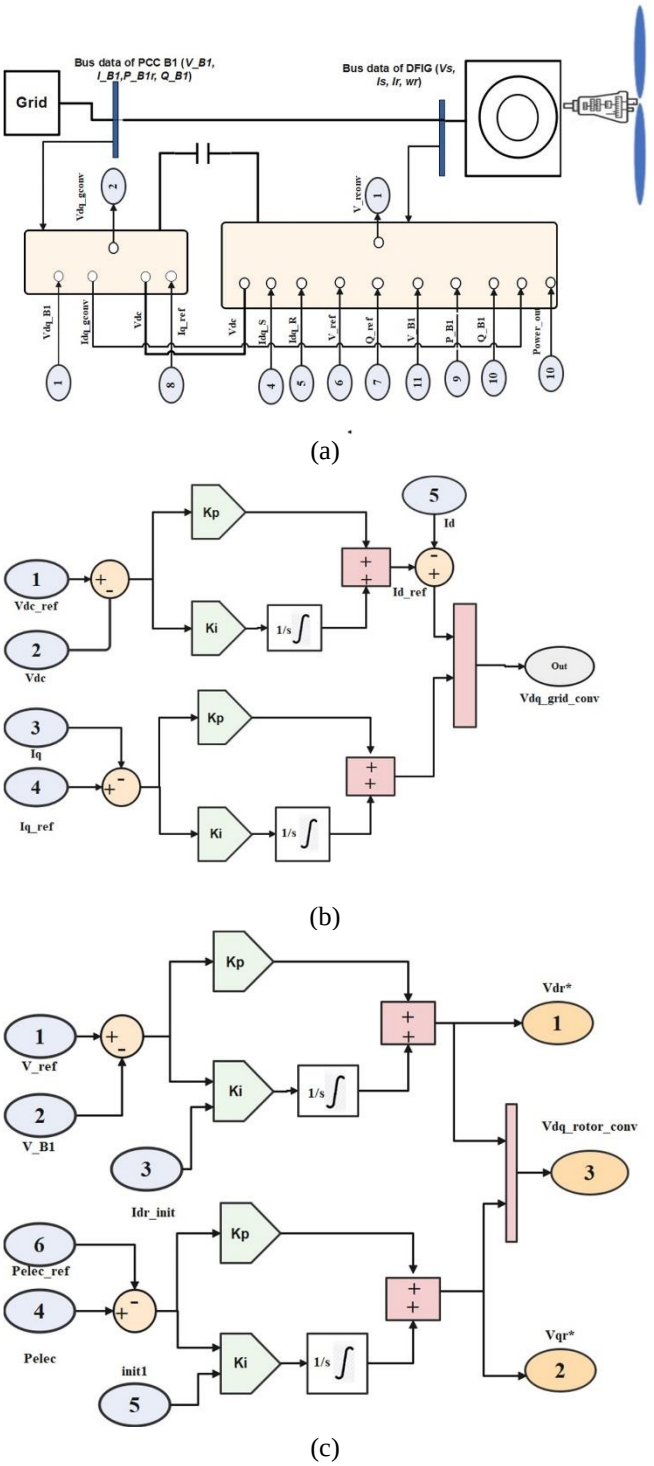

FIGURE 2. (a) The construction of the DFIG PI control system, (b) Grid side PI control system, (c) Rotor side PI control system.

Figure 2 (b) and Figure 2 (c) show the grid and rotor side PI control system of grid and rotor converters. In this paper, two types of controls will be compared (PI control and OSSMC-PI control). The input and output signals of each converter are the same in the two types of controls. In steady state condition, the active power of DFIG can be expressed using

d-q transformation of stator voltage and rotor current as shown [36-39]:

$$\boldsymbol{P_s} = \left(\frac{\boldsymbol{1.5 L_m V_{qs}}}{\boldsymbol{L_s}}\right) \times \boldsymbol{i_{qr}} \quad (22)$$

$$\boldsymbol{P_s} = \boldsymbol{\alpha} \times \boldsymbol{i_{qr}} \quad (23)$$

In which

$$\boldsymbol{\alpha} = \left(\frac{\boldsymbol{L_s}}{\boldsymbol{1.5 L_m V_{qs}}}\right) \quad (24)$$

$$\boldsymbol{i_{qr}} = \boldsymbol{\alpha} \times \boldsymbol{P_s} \quad (25)$$

The deviation of P_s from the reference of the active power (P_{ref}) due to any disturbance (F) will be the error signal of power. The reference of active power will be equal to the optimum power (P_{opt}) which can be obtained from the power characteristic curve of WT. The error power function (e_p) can be given by:

$$\boldsymbol{e_p} = \boldsymbol{P_{opt}} - \boldsymbol{P_s} \quad (26)$$

Many researches had used the equation of error power function (e_p) to present different types of DFIG controls such as in [36, 39]. Even though, SMC had been used in [36, 39], but it depend on the value of (α) in equations (16, 17) to design the switching function (S). Also, as shown in Figure 2 (c), the (e_p) signal represented in equation (26) is the control signal of RSC which controls the rotor voltage of DFIG (V_{rconv}) only. From equations (24), and (25), it can be observed that the value of (α) is dependent on the value of (V_{qs}). This means that any severe turbulence in value of (V_{qs}) and accordingly the value of (α) will influence the control system.

b) The Proposed Optimized Seconded Order SMC-PI Control (OSSMC-PI)

As it is cleared in previous subtitles, DFIG control consists of two impressive signals V_{gconv}, V_{rconv} and V_{rconv}. In addition, the value of V_{qs} and α will influence the control system. This proposed control system (OSSMC-PI) is based on three bases which can be described as follows:

1) Using the advantage of SMC to stabilize systems regardless of external perturbations and unexpected changes in system parameters.
2) Using optimization technique to find the optimum value of (α);
3) Find the optimum value of PI gains ($k_p$and k_i) not only in converter of rotor side but also in converter of grid side using (k_p and k_i).

Figure 3 shows the flowchart of (OSSMC-PI). In (OSSMC-PI), the SMC is applied to both grid and rotor converters. Hence, not only is the error of power represented in (OSSMC-PI) but also, the error signals of DC and AC voltages. The validation of the OSSMC-PI means using the optimized values of the gains to the proposed controller under the system faults. The equations represent the error signals of rotor side converters are given by Eqs. (27) and (28), while Eq. (29) represent the error signal of grid side converters:

$$\boldsymbol{e_{p-rsc}} = \boldsymbol{P_{ref}} - \boldsymbol{P_F} \quad (27)$$

$$\boldsymbol{e_{v-rsc}} = \boldsymbol{V_{ref}} - \boldsymbol{V_F} \quad (28)$$

$$\boldsymbol{e_{vdc-gsc}} = \boldsymbol{V_{dc-ref}} - \boldsymbol{V_{DC-F}} \quad (29)$$

The values of P_F, V_F and V_{DC-F}represent the measured power, AC voltage, DC voltage during disturbance. The values of P_{ref} , V_{ref} and V_{dc-ref} represent the measured power, AC voltage, DC voltage references.

FIGURE 3. the Flowchart of proposed OSSMC-PI

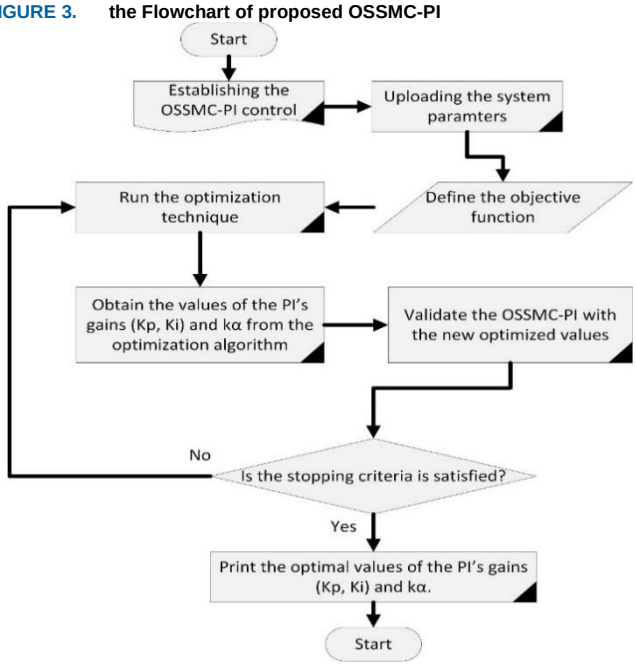

- *Execute the OSSMC-PI on the converter of grid side*

The OSSMC-PI of GSC is presented in Figure 4. The voltage of grid side converter is expressed as:

$$\boldsymbol{V_{dq-gsc}} = \boldsymbol{V_{d-gsc}} + \boldsymbol{jV_{q-gsc}} \quad (30)$$

V_{d-gsc} and V_{q-gsc} are the direct and quadratic components of the voltage of GSC V_{dq-gsc}. The next equations represent the V_{d-gsc} and V_{q-gsc} under the effect of (OSSMC-PI).

$$\boldsymbol{V_{d-gsc}} = \boldsymbol{e_{vdc-gsc}K_p} + \boldsymbol{K_i}\int \boldsymbol{e_{vdc-gsc}dt} - \boldsymbol{F_d} + \boldsymbol{\alpha_{dc-gsc}g_{SMC}} \quad (31)$$

To define the stat space equation let $\boldsymbol{x_1}$ equal to $\int e_{vdc-gsc}d\tau$ and x_2 equal to $e_{vdc-gsc}$ so that the stat space equation can be donated by:

$$\begin{cases} \boldsymbol{x_1} = \boldsymbol{x_2} = \boldsymbol{e_{vdc-gsc}} \\ \boldsymbol{x_2} = -\boldsymbol{x_2K_p} - \boldsymbol{K_i x_1} - \boldsymbol{\alpha_{dc-gsc}g_{SMC}} - \boldsymbol{F_d} \end{cases} \quad (32)$$

FIGURE 4. OSSMC-PI of grid side converter

The equation represents switching to sliding surface are denoted as follows:

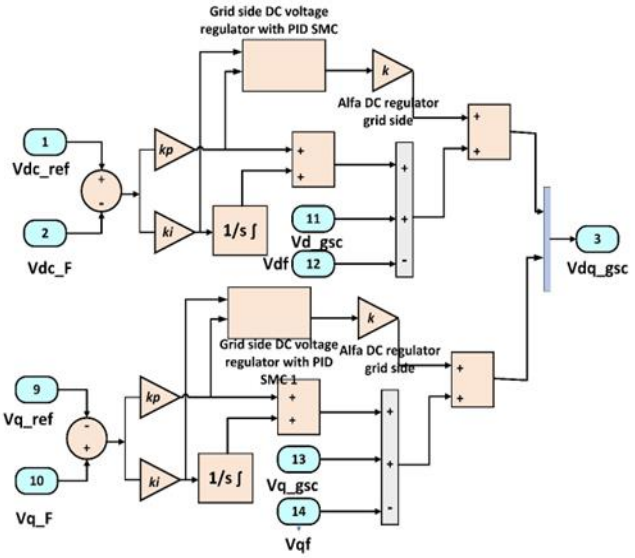

$$S = x_2 + C * x_1 \quad (33)$$

$$\dot{S} = C * x_2 - x_2 K_p - K_i x_1 - \alpha_{dc-gsc} g_{SMC} - F_d \quad (34)$$

$$\dot{S} = x_2 (C - K_p) - K_i x_1 - \alpha_{dc-gsc} g_{SMC} - F_d \quad (35)$$

In the previous equation g_{SMC} can guarantee that the system will slide on the surface if g_{SMC} composed of two parts as shown:

$$g_{SMC} = g_{SMC1} + g_{SMC2} \quad (36)$$

where g_{SMC1} is the sliding condition and g_{SMC2} is used to reduce the chattering effect. Both g_{SMC1} and g_{SMC2} can be expressed as follows:

$$S = x_2 + C * x_1 \quad (37)$$

$$\dot{S} = C * x_2 - x_2 K_p - K_i x_1 - \alpha_{dc-gsc} g_{SMC} - F_d \quad (38)$$

$$\dot{S} = x_2 (C - K_p) - K_i x_1 - \alpha_{dc-gsc} g_{SMC} - F_d \quad (39)$$

So that by substituting equation (36) in equation (31), the direct component of the voltage of grid side converter can be written as follows:

$$V_{d-gsc} = e_{vdc-gsc} K_p + K_i \int e_{vdc-gsc} dt - F_d + \alpha_{dc-gsc} (g_{SMC1} + g_{SMC2}) \quad (40)$$

Likewise, V_{q-gsc} can be obtained using (41).

$$V_{q-gsc} = e_{q-gsc} K_p + K_i \int e_{q-gsc} dt - F_q + \alpha_{dc-gsc} (g_{SMC1} + g_{SMC2}) \quad (41)$$

where e_{q-gsc} is error between the reference quadratic component of the current and the measured current during disturbance and it is given by:

$$e_{q-gsc} = I_{q-ref} - I_{q-F} \quad (42)$$

From equations (33) and (34), the optimum value of *Vd-gsc* and V_{d-gsc} and hence the value of grid side converter V_{dq-gsc} will be occurred when the optimum value ($\alpha_{dc-gsc} - k_i - k_p$) which are obtained using optimization methods.

- *Execute the OSSMC-PI on the RSC*

The OSSMC-PI of RSC is depicted in Figure 5. The converter of rotor side is composed of power regulator and voltage regulator which produces direct component of the voltage of RSC while the power regulator produces quadratic component of the voltage of RSC. The voltage of rotor side converter can be expressed as follows:

$$V_{dq-rsc} = V_{d-rsc} + jV_{q-rsc} \quad (43)$$

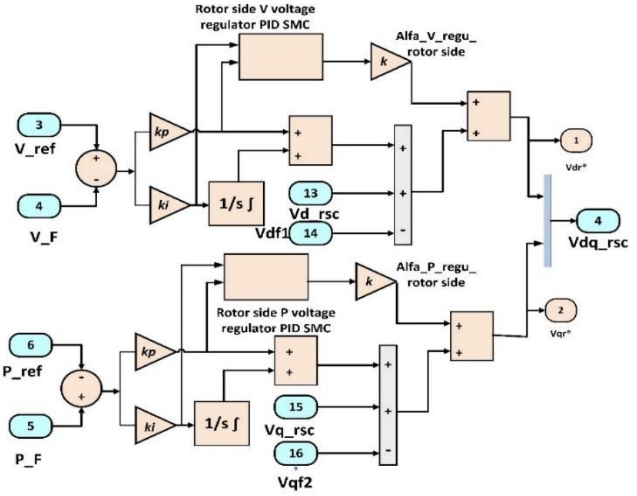

FIGURE 5. **The OSSMC-PI of RSC.**

The value of V_{d-rsc} is produced by voltage regulator and it depends on error signal e_{v-rsc} between the measured voltage during fault V_F and reference voltage V_{ref} as depicted in equation (28). On other hand, the value of V_{q-rsc} is produced by power regulator and it depends on error signal e_{p-rsc} between the measured power during fault P_F and reference power P_{ref} according to (27). Likewise, in grid side converter, the following equations represent the V_{d-rsc} and V_{q-rsc} under the effect of OSSMC-PI.

$$V_{d-rsc} = e_{v-rsc} K_{p-v} + K_{i-v} \int e_{v-rsc} dt - F_v + \alpha_{v-rsc} (g_{SMC3} + g_{SMC4}) \quad (44)$$

$$V_{q-gsc} = e_{p-rsc} K_{p-p} + K_{i-p} \int e_{p-rsc} dt - F_p + \alpha_{p-gsc} (g_{SMC5} + g_{SMC6}) \quad (45)$$

According to equations (44), the optimum value of V_{d-rsc} of voltage regulator can be assigned when the optimum values of

(α_{v-rsc}–K_{i-v}–K_{p-v}) are determined from the optimization methods.

From equations (45), the optimum value of $V_{q-rsc}$of power regulator when the optimum values of (α_{p-rsc}– K_{i-p} –K_{p-p}) are obtained from the optimization methods.

From equations (44)and (45), the optimum value of V_{d-rsc} and V_{q-rsc} are assigned. Sub sequentially, it can provide the optimal control ability of rotor side converter including the voltage regulator and power regulator via optimum values of (α_{v-rsc} – K_i –K_p).

III. GULF OF EL ZAYT WIND FARM

Gulf El-Zayt wind farm is large Egyptian wind energy power plants which is considered a largest wind energy project in the Middle East. The Gulf El-Zayt wind farm has a total capacity is 580 MW that is connected in three stages. The first stage is 240 MW (2MW*120 wind turbines) while the second stage is 220 MW (2MW *110 wind turbines) and the third stage is 120 MW (2*60). The type of the WT is Gamesa G80 in which its rated capacity is 2000 kW while the cut-in (V_{in}), cut-out (V_{out}), and the rated (V_r), wind speeds are listed in Table 1. The power

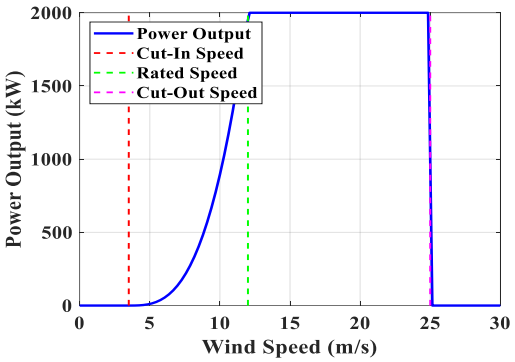

generated by the WT v.s. the wind speed variations are depicted in Figure 6 [40].

FIGURE 6. Gamesa-80 turbine wind speed.

TABLE I
SPECIFICATION OF THE WT

Parameter	Value
Rated power (kW)	2000
V_{in} (m/s)	3.5
V_r (m/s)	12
V_{out} (m/s)	25
R (m)	80
$Area$ (m2)	5.027
Blade length (m)	37
Height of the hub (m)	100

IV. OPTIMIZATION

A. SLIME MOULD ALGORITHM

The SMA is an efficient bio-based algorithm that conceptualized from the construction slime mould which depend upon three stage including approach food, Wrap food and the oscillation [20]. The mathematical representation of the SMA is formulated as follows:

1) APPROACH FOOD

The mould goes directly to the location of the food from its odour. This behavior can be represented as follows:

$$\boldsymbol{h(t+1)} = \begin{cases} \boldsymbol{h_b(t) + vb \cdot (W \cdot h_A(t) - h_B(t)), rand < p} \\ \boldsymbol{vc \cdot h(t), rand \geq p} \end{cases} \quad (46)$$

In which

$$\boldsymbol{p = tanh|Fit(i) - DL|} \quad (47)$$

$$\boldsymbol{vb} = [-a, a] \quad (48)$$

$$\boldsymbol{a = arctanh\left(-\left(\frac{t}{T_{max}}\right) + 1\right)} \quad (49)$$

$$\boldsymbol{W(SI(i))} = \begin{cases} \boldsymbol{1 + r \cdot log\left(\frac{bF - S(i)}{bF - wF} + 1\right)}, condition \\ \boldsymbol{1 - r \cdot log\left(\frac{bF - S(i)}{bF - wF} + 1\right)}, others \end{cases} \quad (50)$$

$$\boldsymbol{SI = sort(Fit)} \quad (51)$$

where the position of the SM, h_b the best placement of the food, t denotes the current iteration number, T_{max} is the maximum iteration number, SI is the sorting of the objective function values, h_A, and h_B refer to random vectors from the populations, $rand$ is a random factor between 0 and 1, bF is the best objective function, wF is the worst objective function. Fit the corresponding objective function of the h . DL represents the best objective function.

2) WRAP FOOD

Wrap food mimics the venous tissue contraction where the flow of the cytoplasm will be increased due to increasing thickness and the strength of the vein when the concentration of the food and the bio-oscillator are high. The wrap food phase can be represented as follows:

$$\boldsymbol{h^*(t+1)} = \begin{cases} \boldsymbol{rand \times (ub - lb) + lb, rand < z} \\ \boldsymbol{X_b(t) + vb \cdot (W \cdot h_A(t) - h_B(t)), rand < p} \\ \boldsymbol{vc \times h(t), rand \geq p} \end{cases} \quad (52)$$

where z is a constant value. lb refers to the lower limit of the search range while ub is the upper limit.

3) OSCILLATION

The biological oscillator generates signal for changing the cytoplasmic flow to accommodate the location of the mould based on the best location (high concentration) of the food. Thus, the slime mould's venous thickness is varied based on W, vb, and vc. For simulating the oscillation frequency, the W was utilized which depends upon the food concentration. When the quantity of food is high, the SM can go to this food quickly while the slime mould moves slowly when the concentration of food is low. The second and the third parameters that can control the behavior of the slime mould

are vb and vc are oscillated between [-2, 2] and [-1, 1], respectively. The SMA's flow chart is presented in Figure 7.

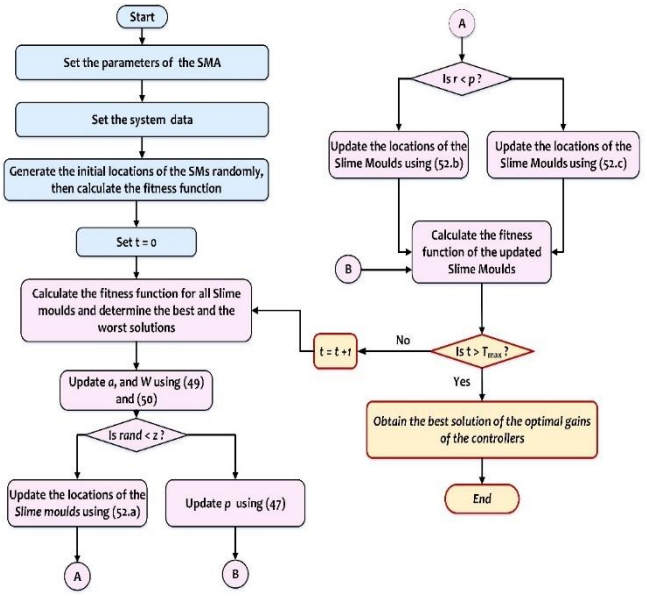

FIGURE 7. **The flow chart of the SMA.**

B. PARTICLE SWARM OPTIMIZATION

Particle swarm optimization algorithm (PSO) is a swam optimization technique that simulates swarm motion of fished or birds which was proposed by James Kennedy and Russell Eberhart [41]. Each solution represents a particle which updates its location based on its experience as well as the experience of neighboring particles. The following steps describe the of the PSO

- Generate the locations of the particles and the corresponding velocities randomly.
- Find the corresponding objective function of each particle.
- Update the velocity of the particles as follows:

$$V_i(t+1) = \omega \times V_i(t) + c_1 \times r1 \times \left(Pbest_i - X_i(t)\right) + c_2 \times r2 \times \left(Gbest - h_i(t)\right) \quad (53)$$

- where $r1$ and $r2$ are random values within [0-1]. c_1 and c_2 are weight factors. $Gbest$ is the best global solution. $Pbest_i$ is the best solution is founded by particle i.
- Update the location of each particle as follows:

$$X_i(t+1) = X_i(t) + V_i(t+1) \quad (54)$$

V. SIMULATION RESULTS AND DISCUSSIONS

Here, the performance of the Gulf of El Zayt wind farm based on DFIG is simulated. In addition, this simulation is studied under the occurrence of grid faults by applying the suggested OSSMC-PI. The results obtained of this simulated case are compared with the application of other controllers. These controllers like the Sliding Mode Controller (SMC) and PI controller. The optimal gains of these controllers have been assigned optimally using the SMA and PSO optimizers. The simulations were conducted on a core I7 PC with CPU 2.9 GHz, 32 GB RAM using MATALB software. In this paper six studied cases are presented which have been depicted as follows: (a) Case1: PI only with SMA, (b) Case 2: PI only with PSO, (c) Case 3: OSSMC-PI with SMA, (d) Case 4: OSSMC-PI with PSO, (e) Case 5: SMC only with SMA, and (f) Case 6: SMA only with PSO. The cases studied and the corresponding optimal gains are listed in Table 2 and Table 3. The optimal parameters that have been determined by the reported algorithms are α_{dc-gsc} , α_{v-rsc}, α_{p-rsc}, K_i and K_p.

TABLE II
THE OPTIMIZED SETTING OF GAINS FOR CASES 1, 2 AND 3.

Regulators		Case1: PI only with SAM		Case2: PI only with PSO		Case3: OSSMC-PI with SMA		
Rotor side converters	Power regulator	K_p	K_i	K_p	K_i	K_p	K_i	α_{v-rsc}
		2	235	0.9678	111.08	0.00103	6.536	3.1548
	AC voltage regulator	K_p	K_i	K_p	K_i	K_p	K_i	α_{v-rsc}
		3.7513	200	7.0418	578.46	1.1847	450.8	4.9847
Grid side converters	DC voltage Regulator	K_p	K_i	K_p	K_i	K_p	K_i	α_{dc-gsc}
		4.15E-4	0.07445	0.022	0.0319	0.0044	0.0724	10

TABLE III
THE OPTIMAL SETTING OF GAINS FOR CASES 4, 5 AND 6.

Regulators		Case 4: OSSMC-PI with PSO			Case 5: Only SMC with SMA	Case 6: Only SMC with PSO
Rotor side converters	Power regulator	K_p	K_i	α_{p-rsc}	α_{p-rsc}	α_{p-rsc}
		1.6145	210	2.675	0.5051	0.7802
	AC voltage regulator	K_p	K_i	α_{v-rsc}	α_{v-rsc}	α_{v-rsc}
		7.689	641.6	4.979	0.0750	0.0601
Grid side converters	DC voltage regulator	K_p	K_i	α_{dc-gsc}	α_{dc-gsc}	α_{dc-gsc}
		0.0079	0.0865	9.578	-0.006	-0.0025

The cases study the performance of the Gulf Elzayt wind farm during a three-phase fault based on 6 types of control. The duration of the fault is 150 ms. The fault occurred 25 seconds after the start of simulation time and after the wind speed reaches its peak speed equal to 14 m/s. The authors chose this operating condition because it represents a harsh situation. Figure 8 (a) displays the effect of wind speed and three-phase condition for all studied cases. It is clearly shown in Figure 8 (a), in all studied cases, the Gulf Elzayt wind farm can remain connected to the network during the increase in wind speed and even when the wind generation units work at maximum wind speed. Hence, the authors focus on the fault period where the measured voltage, active, and reactive powers are at the point connection between the interconnected grid and wind farms. Also, speed, pitch angle, and dc-link voltage are observed. Figure 8 (b) focuses on the impact of fault condition on all studied cases. Figure 8 (b) shows that, just before fault occurrence cases 1, 2, 3 and 4 have the highest value of output power while cases 5 and 6 have the lowest value of output power. During fault conditions, the active power in cases 3, 4, 5, and 6 does not decrease to zero but the WTs are still connected and in service to the electric system. The active power in cases 1, and 2 decreases to zero during the fault and remains at zero output power which means that the wind generation units are disconnected from the main electric system. Figure 8 (b) also shows that the active power of case 4 has reached its steady state much faster than case 5. Also, as exposed in Figure 8 (b) and after fault clearance, the active power of cases 5, and 6 have increased then then suddenly dropped to zero.

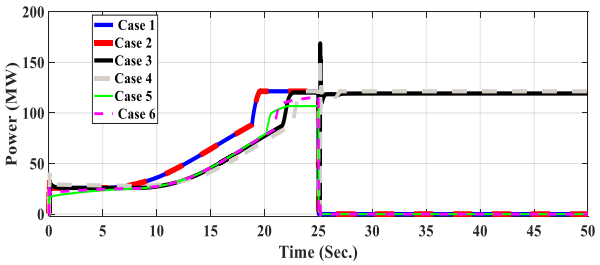

(a)

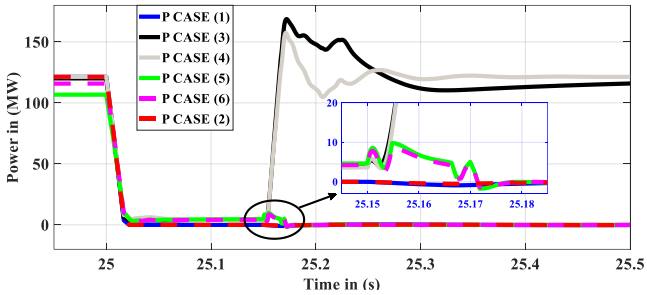

(b)

FIGURE 8. **(a) The active power of the 6 cases during fault condition (b) Zoomed active power.**

The behaviors of active power can be understood by observing the voltage and reactive power curves as illustrated in Figure 9 and Figure 10, respectively. As shown in Figure 6, before fault occurrence the WTs operate at maximum wind speed (cut of speed) which means that there will be significant reactive power absorbed from the system network (Q_{sys}) and a significant amount of reactive power injected from the DC bus of wind farm (Q_{wf}). During the increase of wind speed to maximum speed and before fault occurrence, the voltages of cases 1, 2, 3, and 4 are slightly higher than the voltages of cases 5 and 6. This is due to the delivered reactive power from the network for cases 1, 2, 3, and 4 are lower than absorbed reactive of cases 5 and 6 as shown in Figure 10 (a), and (b), respectively.

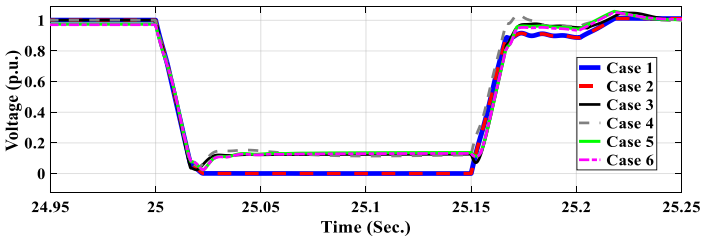

FIGURE 9. **Voltage of the 6 cases.**

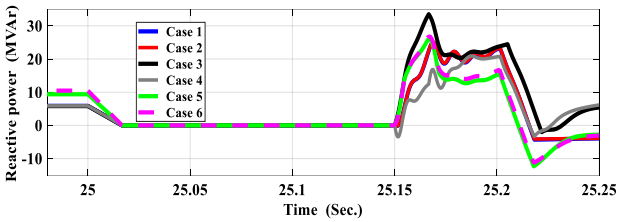

(a)

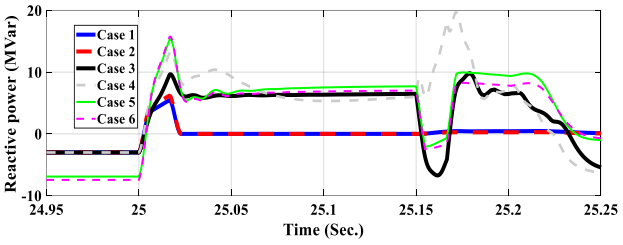

(b)

FIGURE 10. Reactive power of the 6 cases. (a) Reactive power at bus of the grid and (b) Reactive power at bus of the wind farm

As exposed in Figure 9, during the fault cases 1, 2, 3, and 4 have a higher voltage value compared with the voltages of cases 5 and 6. This is because cases 1, 2, 3, and 4 absorb lower reactive power from the grid compared with the reactive power of cases 5 and 6 as displayed in Figure 10 (a) and (b), respectively. In Figure 10 and after fault clearance, the voltage of case 4 has returned to its steady state much faster than the other cases. This explains why the active power of case 4 returns fast to its steady state. The fast return of case 4 voltage to its steady state is due to the increase in an injected reactive power (Q_{wf}) as displayed in Figure 10 (b). Also, this fast return to the steady state of case 4 will cause a decrease in system reactive power (Q_{sys}) as displayed in Figure 10 (a).
The injected DC bus voltages of the 6 cases are displayed in Figure 11. From Figure 11, the DC voltages of cases 5 and 6 have the highest voltage values before and during fault. After fault clearance at time equal to 25.15 second the DC voltages of cases 5 and, 6 are still high which will cause disconnection of wind farm at time equal to 25.17 second as shown in Figure 8 (b). On other hand, after fault clearance the DC voltages of cases 3 and, 4 have decreased which will guarantee the contentious connection of wind farm. Due to the disconnection the DC voltages of cases 1 and 2 remains constant at its rated value

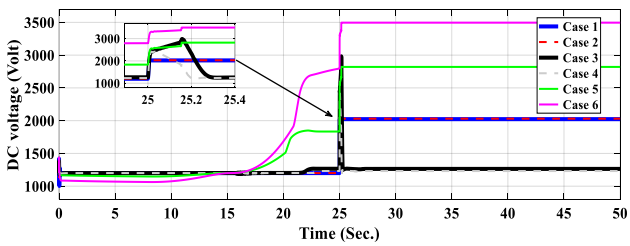

FIGURE 11. DC voltage for the 6 cases.

The speed of the rotor and pitch angle are displayed in Figure 12, and Figure 13 for the 6 cases. These figures prove the disconnection of wind farm of cases 1, 2, 5 and, 6 where their speed of rotor and pitch angle become out of synchronization. On the contrary, the pitch angle and the velocity of rotor of cases 3 and, 4 have returned to their steady state and keep the contentious connection of wind farm.

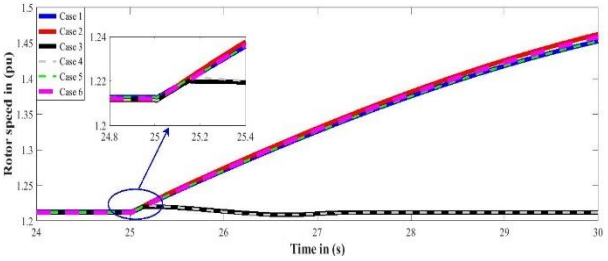

FIGURE 12. Rotor speed for the 6 cases.

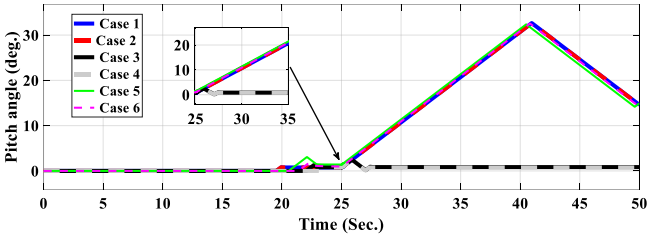

FIGURE 13. Pitch angle of the 6 cases.

VI. CONCLUSION

In this paper an improved Seconded Order Sliding Mode Control (SSMC) has been investigated. This was achieved by optimizing the corresponding gains of SSMC including α_{p-rsc} and α_{p-rsc} of the power regulator, AC voltage regulator and DC voltage regulator. Also, the gains of PI including K_p, and K_i of the power regulator, AC voltage regulator and DC voltage regulator has been obtained by application the optimization methods. The optimized SSMC-PI (OSSMC-PI) has been applied and tested on the Gulf El-Zayt wind farm. The performance of the Gulf El-Zayt wind farm based on this proposed method (OSSMC-PI) was examined during a three-phase fault in six different cases; Case1: Only PI with SMA, Case2: Only PI with PSO, Case3: (PI +SMC) with SMA, Case3: (PI +SMC) with SMA, Case4: (PI +SMC) with PSO, Case5: Only SMC with SMA and, Case6: Only SMC with PSO. As per the obtained results, the best results occurred in cases 3 and 4 where the proposed method (OSSMC-PI) was applied. In addition to that the OSSMC-PI can improve the performance and reliability of Gulf El-Zayt wind farm during the surge operating conditions such as three-phase faults. All of these results prove that the viewpoint of the paper which depends on using optimization

to determine the value of gain (α) in the equation of Seconded Order Sliding Mode Control can improve the performance and reliability of Gulf El-Zayt wind farm.

REFERENCES

[1] M. Ebeed, O. NourEldeen, and A. Ebrahim, "Assessing Behavoir of the Outer Crowbar Protection with the DFIG during Grid Fault," in *2nd Int. Conf. Energy Syst. Technol*, 2013, pp. 18-21.

[2] W. e. strategy. Available: http://www.nrea.gov.eg/

[3] H. Jadhav and R. Roy, "A comprehensive review on the grid integration of doubly fed induction generator," *International Journal of Electrical Power & Energy Systems*, vol. 49, pp. 8-18, 2013.

[4] P. Catalán, Y. Wang, J. Arza, and Z. Chen, "A comprehensive overview of power converter applied in high-power wind turbine: Key challenges and potential solutions," *IEEE Transactions on Power Electronics*, vol. 38, no. 5, pp. 6169-6195, 2023.

[5] A. A. Chhipą *et al.*, "Modeling and control strategy of wind energy conversion system with grid-connected doubly-fed induction generator," *Energies*, vol. 15, no. 18, p. 6694, 2022.

[6] C. Raghavendran, J. P. Roselyn, and D. Devaraj, "Development and performance analysis of intelligent fault ride through control scheme in the dynamic behaviour of grid connected DFIG based wind systems," *Energy Reports*, vol. 6, pp. 2560-2576, 2020.

[7] B. Desalegn, D. Gebeyehu, and B. Tamrat, "Evaluating the performances of PI controller (2DOF) under linear and nonlinear operations of DFIG-based WECS: A simulation study," *Heliyon*, vol. 8, no. 12, 2022.

[8] L. Xiong, P. Li, and J. Wang, "High-order sliding mode control of DFIG under unbalanced grid voltage conditions," *International Journal of Electrical Power & Energy Systems*, vol. 117, p. 105608, 2020.

[9] A. Merabet, H. Eshaft, and A. A. Tanvir, "Power-current controller based sliding mode control for DFIG-wind energy conversion system," *IET Renewable Power Generation*, vol. 12, no. 10, pp. 1155-1163, 2018.

[10] Y. Liu *et al.*, "DFIG wind turbine sliding mode control with exponential reaching law under variable wind speed," *International Journal of Electrical Power & Energy Systems*, vol. 96, pp. 253-260, 2018.

[11] P. Li, L. Xiong, F. Wu, M. Ma, and J. Wang, "Sliding mode controller based on feedback linearization for damping of sub-synchronous control interaction in DFIG-based wind power plants," *International Journal of Electrical Power & Energy Systems*, vol. 107, pp. 239-250, 2019.

[12] K. Elyaalaoui, M. Labbadi, M. Ouassaid, M. Cherkaoui, and M. Bouzi, "High-order sliding-mode control using integral terminal sliding manifold for a wind turbine under grid faults," *International Journal of Control*, vol. 97, no. 3, pp. 635-650, 2024.

[13] B. Beltran, M. E. H. Benbouzid, and T. Ahmed-Ali, "Second-order sliding mode control of a doubly fed induction generator driven wind turbine," *IEEE Transactions on Energy Conversion*, vol. 27, no. 2, pp. 261-269, 2012.

[14] X. Liu, Y. Han, and C. Wang, "Second-order sliding mode control for power optimisation of DFIG-based variable speed wind turbine," *IET Renewable Power Generation*, vol. 11, no. 2, pp. 408-418, 2017.

[15] L. Saihi, Y. Bakou, A. Harrouz, M. Boura, I. Colak, and K. Kayisli, "Fuzzy-sliding mode control second order of wind turbine based on DFIG," in *2022 10th International Conference on Smart Grid (icSmartGrid)*, 2022, pp. 296-300: IEEE.

[16] C. Evangelista, F. Valenciaga, and P. Puleston, "Active and reactive power control for wind turbine based on a MIMO 2-sliding mode algorithm with variable gains," *IEEE Transactions on Energy Conversion*, vol. 28, no. 3, pp. 682-689, 2013.

[17] S. Ebrahimkhani, "Robust fractional order sliding mode control of doubly-fed induction generator (DFIG)-based wind turbines," *ISA transactions*, vol. 63, pp. 343-354, 2016.

[18] K. Liao, Z. He, Y. Xu, G. Chen, Z. Y. Dong, and K. P. Wong, "A sliding mode based damping control of DFIG for interarea power oscillations," *IEEE Transactions on Sustainable Energy*, vol. 8, no. 1, pp. 258-267, 2016.

[19] L. Saihi, B. Berbaoui, and Y. Bakou, "Sliding Mode of Second-Order Control Based on Super-Twisting ANFIS Algorithm of Doubly Fed Induction Generator in Wind Turbines Systems with Real Variable Speeds," *Iranian Journal of Science and Technology, Transactions of Electrical Engineering*, vol. 47, no. 2, pp. 473-490, 2023.

[20] S. Li, H. Chen, M. Wang, A. A. Heidari, and S. Mirjalili, "Slime mould algorithm: A new method for stochastic optimization," *Future generation computer systems*, vol. 111, pp. 300-323, 2020.

[21] M. Abdel-Basset, V. Chang, and R. Mohamed, "HSMA_WOA: A hybrid novel Slime mould algorithm with whale optimization algorithm for tackling the image segmentation problem of chest X-ray images," *Applied soft computing*, vol. 95, p. 106642, 2020.

[22] L. Liu *et al.*, "Performance optimization of differential evolution with slime mould algorithm for multilevel breast cancer image segmentation," *Computers in Biology and Medicine*, vol. 138, p. 104910, 2021.

[23] C. Kumar, T. D. Raj, M. Premkumar, and T. D. Raj, "A new stochastic slime mould optimization algorithm for the estimation of solar photovoltaic cell parameters," *Optik*, vol. 223, p. 165277, 2020.

[24] M. Mostafa, H. Rezk, M. Aly, and E. M. Ahmed, "A new strategy based on slime mould algorithm to extract the optimal model parameters of solar PV panel," *Sustainable Energy Technologies and Assessments*, vol. 42, p. 100849, 2020.

[25] M. H. Hassan, S. Kamel, L. Abualigah, and A. Eid, "Development and application of slime mould algorithm for optimal economic emission dispatch," *Expert Systems with Applications*, vol. 182, p. 115205, 2021.

[26] Y. M. Wazery, E. Saber, E. H. Houssein, A. A. Ali, and E. Amer, "An efficient slime mould algorithm combined with k-nearest neighbor for medical classification tasks," *IEEE Access*, vol. 9, pp. 113666-113682, 2021.

[27] J. Hu *et al.*, "Dispersed foraging slime mould algorithm: Continuous and binary variants for global optimization and wrapper-based feature selection," *Knowledge-Based Systems*, vol. 237, p. 107761, 2022.

[28] D. İzci and S. Ekinci, "Comparative Performance Analysis of Slime Mould Algorithm For Efficient Design of Proportional-Integral-Derivative Controller," *Electrica*, vol. 21, no. 1, 2021.

[29] S. Khunkitti, A. Siritaratiwat, and S. Premrudeepreechacharn, "Multi-objective optimal power flow problems based on slime mould algorithm," *Sustainability*, vol. 13, no. 13, p. 7448, 2021.

[30] X. Liang, D. Wu, Y. Liu, M. He, and L. Sun, "An enhanced slime mould algorithm and its application for digital IIR filter design," *Discrete Dynamics in Nature and Society*, vol. 2021, pp. 1-23, 2021.

[31] D. Agarwal and P. S. Bharti, "Implementing modified swarm intelligence algorithm based on Slime moulds for path planning and obstacle avoidance problem in mobile robots," *Applied Soft Computing*, vol. 107, p. 107372, 2021.

[32] A. Kasbi and A. Rahali, "A simple methodology for optimal fuzzy control of DFIG based wind turbine," in *2020 1st International Conference on Innovative Research in Applied Science, Engineering and Technology (IRASET)*, 2020, pp. 1-6: IEEE.

[33] A. Kasbi and A. Rahali, "Performance improvement of modern variable-velocity wind turbines technology based on the doubly-fed induction generator (DFIG)," *Materials Today: Proceedings*, vol. 45, pp. 5426-5432, 2021.

[34] M. Shahbazi, P. Poure, S. Saadate, and M. R. Zolghadri, "Five-leg converter topology for wind energy conversion system with doubly fed induction generator," *Renewable Energy*, vol. 36, no. 11, pp. 3187-3194, 2011.

[35] O. Soares, H. Gonçalves, A. Martins, and A. Carvalho, "Nonlinear control of the doubly-fed induction generator in wind power systems," *Renewable Energy*, vol. 35, no. 8, pp. 1662-1670, 2010.
[36] S. Li, H. Wang, Y. Tian, A. Aitouch, and J. Klein, "Direct power control of DFIG wind turbine systems based on an intelligent proportional-integral sliding mode control," *ISA transactions*, vol. 64, pp. 431-439, 2016.
[37] A. Rashad, S. Kamel, F. Jurado, and S. H. Abdel Aleem, "Stability of distribution networks with wind turbines," *Electric Distribution Network Management and Control*, pp. 281-308, 2018.
[38] A. Rashad, S. Kamel, and F. Jurado, "The basic principles of wind farms," *Distributed Generation Systems*, pp. 21-67, 2017.
[39] A. Rashad, S. Kamel, F. Jurado, M. Rihan, and M. Ebeed, "Optimal design of SSSC and crowbar parameters for performance enhancement of Egyptian Zafrana wind farm," *Electrical Engineering*, pp. 1-17, 2022.
[40] *Wind turbine data*. Available: https://www.thewindpower.net/turbine_en_44_gamesa_g80-2000.php
[41] J. Kennedy and R. Eberhart, "Particle swarm optimization," in *Proceedings of ICNN'95-international conference on neural networks*, 1995, vol. 4, pp. 1942-1948: ieee.

MOHAMED EBEED received the B.S. degree from Aswan University, Egypt, in 2005, the M.S. degree in electrical engineering from South Valley University, in 2013, and the jointly-supervised Ph.D. degree from the Department of Electrical Engineering, Faculty of Engineering, Aswan University, and the University of Jaén, Spain, in 2018. From 2008 to 2009, he was a Lecturer with the Aswan Technical Institute. From 2009 to 2017, he was a Maintenance Engineer with EFACO Company. He is currently an Assistant Professor with the Department of Electrical Engineering, Faculty of Engineering, Sohag University, Egypt.

NAGWA ELBADRY received the BSc from Faculty of Engineering, AL-Azhar University, Egypt in 2018. She is currently pursuing her MSc degree in Department of Electrical Engineering, Sohag Faculty of Engineering, Sohag University. Her research activities include renewable energy and optimization.

KHAIRY SAYED (Member, IEEE) received the B.S. degree in electrical power and machines from Assiut University, Assiut, Egypt, in 1997, the master's degree from the Electrical Energy Saving Research Center, Graduate School of Electrical Engineering, Kyungnam University, Masan, South Korea, in 2007, and the Ph.D. degree from Assiut University, in 2013. He is currently an Associate Professor with the Department of Electrical Engineering, Sohag University, Egypt. His research interests include soft-switching dc–dc power converter topologies, high-frequency inverter applications, renewable energy-related power conditioners, and control schemes. He received the Best Student Paper Award from the 57th Annual Conference of the International Appliances Technical Conference IATC2006 held at Crowne Plaza, Chicago, IL, USA, March 27– 29, and Sohag University Encouragement Awards in the field of engineering science, from 2016 to 2017.

AHMED RASHAD received the B.Eng. from Faculty of Energy Engineering, Aswan University, Egypt and M.Sc. degree in electrical power engineering from Faculty of Engineering, South Valley University, Egypt in 2013. He received the jointly supervised PhD degree in Department of Electrical Engineering, Aswan Faculty of Engineering, Aswan University, Egypt and University of Jaen, Spain in 2018. His research activities include Power system modeling, analysis and simulation, renewable energy and smart grid technologies, applications of power electronics to power systems and power quality.

SULAIMAN Z. ALMUTAIRI was born in 1988. He received the B.Sc. degree from Prince Sattam Bin Abdulaziz University, Al-Kharj, Saudi Arabia, in 2012, and the M.Sc. and Ph.D. degrees from the University of South Florida, Tampa, FL, USA, in 2016 and 2021, respectively. He is currently an Assistant Professor with Prince Sattam Bin Abdulaziz University.

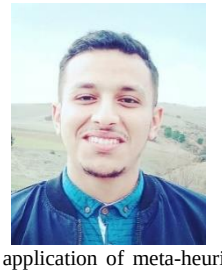

AHMED HACHEMI was born in Laghouat, Algeria. He received his B.Sc. degree in Electrical Engineering from the University Amar Telidji, Laghouat, Algeria, in 2018, and his M.Sc. degree in Electrical Engineering from the same university in 2020. He obtained his Ph.D. degree in Electrical Engineering from the University of Kasdi Merbah Ouargla, Algeria, in 2024. His research interests encompass various aspects of electrical engineering, including the application of meta-heuristic methods in distribution power systems and smart grids, renewable energy generation, DSTATCOMs, and BESS.

EMAD A. MOHAMED received the B.Sc. and M.Sc. degrees in electrical power engineering from Aswan University, Aswan, Egypt, in 2005 and 2013, respectively, and the Ph.D. degree in electrical power engineering from the Kyushu Institute of Technology, Japan, in 2019.,He was a Demonstrator with the Department of Electrical Engineering, Aswan Faculty of Engineering, Aswan University, from November 2007 to August 2013, and an Assistant Lecturer, from 2013 to 2015. He was a Research Student with Kyushu University, Japan, from April to October 2015. He was in a Master Mobility Scholarship at the Faculty of Sciences and Technology, University of Nancy, Lorraine, France. He has been an Assistant Professor at the Faculty of Engineering, Aswan University, since 2019. His current research interests include applications of superconducting power devices, power system control, stability, reliability, and protection.

SHAZLY A. MOHAMED was born in the Red Sea, Egypt. He received the B.Sc. degree in electrical power and machines engineering from Minia University, Minia, Egypt, in 2005, the Master of Science and Doctor of Philosophy (Ph.D.) in Electrical Power Engineering, Faculty of Engineering according to the channel system between Pontificia de Comillas University in Madrid (Spain) & South Valley University (Egypt) in 2011 and 2014 respectively. He has an Associate Professor with the Department of Electrical Engineering, Faculty of Engineering, South Valley University, Qena, Egypt, since 2020 till now. His research interests include renewable energy sources, especially wind energy issues, power electronics, micro grid, and power quality.